ROYAL SOCIETY
OF CHEMISTRY

RESEARCH ARTICLE

Check for updates

Novel lithocholic acid-diindolylmethane hybrids as potent sialyltransferase inhibitors targeting triple-negative breast cancer: a molecular hybridization approach

Christian Angelo P. Concio, [iD] [abc] Ser John Lynon P. Perez, [iD] [ac] Tzu-Ting Chang,[a] Chia-Ling Chen,[c] Yi-Ting He,[cf] Susan D. Arco*[b] and Wen-Shan Li [iD] *[acdef]

Molecular hybridization, an emerging strategy for the discovery of new anticancer therapeutics, shows promise as a powerful tool for the development of new sialyltransferase (ST) inhibitors for cancer treatment. This concept inspired the design of novel ST inhibitors through the hybridization of lithocholic acid and diindolylmethane, leading to the discovery of LCA-DIM hybrids as potential chemical entities targeting STs. Preliminary screening revealed the significance of the DIM moiety and incorporation of Asp linker on enhancing the inhibitory activity and selectivity of the hybrids towards ST6GAL1, inhibiting up to 100% of ST6GAL1 activity at 25 μM with no ST3GAL1 inhibition even at 500 μM. Incorporation of various 5,5′-substituents enhanced the inherent antimigration properties of the hybrids, with **IAN-5B** (R = Cl) and **IAN-15B** (R = N_3) presenting the highest antimigration activity across several triple-negative breast cancer (TNBC) cell lines (MDA-MB-231, BT549, Hs578T) and considerable antiangiogenetic effect by suppressing HUVEC tube formation. This could be attributed to the excellent ST6GAL1 inhibitory activities of the two hybrids with IC_{50} values of 6.6 ± 0.2 μM and 3.3 ± 0.1 μM, respectively. Overall, this study highlights LCA-DIM hybrids as novel, potent, and *N*-glycan-selective ST inhibitors with promising antimigration properties against aggressive TNBC.

1. Introduction

Sialic acids are a diverse group of nine-carbon monosaccharides typically found at the terminal ends of cell surface glycoproteins, where they play essential roles in numerous biological functions. Sialylation induces morphological changes in the cellular surface, resulting in the stabilization of enzymes and hormones, as well as mediating interactions with other neighboring cells. Furthermore, sialic acids serve as ligands for glycan-binding proteins such as selectins, galectins, and siglecs,

establishing their critical role in cellular interactions and cell-to-cell recognition.[1–3] Although essential for normal cellular functions, this post-translational modification is often exploited by various carcinomas, resulting in hypersialylation — characterized by the excessive accumulation of sialic acids on the cancer cell surface. Extensive studies have established the direct association between hypersialylation and cancer progression and metastasis. For instance, hypersialylation is known to impair cancer cell adhesion at the primary tumor site and promote the epithelial-to-mesenchymal transition (EMT).[4–6] Additionally, this process also enables cancer cells to evade immune surveillance and resist apoptosis by mimicking essential glycan motifs.[3,6,7] Despite the significant challenges in targeting hypersialylation, the enzyme sialyltransferase plays a pivotal role in this process and remains a critical target for ongoing research.

Sialyltransferase (ST) is a key regulator of the sialylation pathway responsible for transferring the sialic acid group from CMP-Neu5Ac to the terminal hydroxyl groups of glycoproteins or glycolipids, thereby its upregulation contribute to the abnormal sialic acid accumulation seen in hypersialylation.[1,8] To date, a variety of human STs have already been discovered, demonstrating diversity in their preferred sugar substrates, type

[a] *Biomedical Translational Research Center, Academia Sinica, No. 99, Lane 130, Section 1, Yanyuan Road, Nangang District, Taipei City 115, Taiwan. E-mail: wenshan@as.edu.tw*
[b] *Institute of Chemistry, College of Science, University of the Philippines Diliman, Quezon City, Metro Manila, Philippines*
[c] *Institute of Chemistry, Academia Sinica, No. 128, Section 2, Yuanyuan Road, Nangang District, Taipei City 115, Taiwan*
[d] *Doctoral Degree Program in Marine Biotechnology, National Sun Yat-Sen University, Kaohsiung 804, Taiwan*
[e] *PhD Program in Biotechnology Research and Development, Taipei Medical University, Taipei 115, Taiwan*
[f] *Department of Medicinal and Applied Chemistry, Kaohsiung Medical University, Kaohsiung 807, Taiwan*

of glycosidic linkage formed, and specificity for *N*-glycans or *O*-glycans. Interestingly, specific ST isozymes have been shown to be overexpressed and play a key role in promoting hypersialylation in multiple carcinomas including breast,[9,10] ovarian,[11–13] pancreatic,[12,14,15] and colorectal cancer,[16,17] positioning the inhibition of ST isozymes with high potency and selectivity as a promising therapeutic strategy for these malignancies.

Although there is a rising attention towards the therapeutic applications of sialyltransferase for cancer treatment, only a few compounds capable of effectively inhibiting ST activity have been recorded,[18–20] emphasizing the need for the exploration of novel and more potent ST inhibitors. Notably, molecular hybridization has emerged as a promising strategy in drug discovery given the vast array of available structural motifs with advantageous pharmacological properties. In the context of ST inhibitors, lithocholic acid (LCA) has been highlighted as a key motif, leading to the discovery of potent ST inhibitors such as Lith-O-Asp (see Fig. 1). Both LCA-based structures have demonstrated significant antiangiogenic and antimetastatic effects in lung carcinoma *in vitro* and *in vivo*.[21–23] Utilization of this steroidal motif also resulted in the development of first ever recorded *N*-glycan selective ST inhibitors such as FCW34,[24] FCW393 (ref. 25) and SPP-002,[26] capable of inhibiting melanoma and/or breast cancer progression. Interestingly, recent exploration of the LCA core suggests the importance of indole[27,28] and indole-like[29] moieties for ST inhibition activity, a trend also observed in other proposed ST inhibitors. Motivated by this, we surveyed various indole-containing metabolites for integration into the LCA core to enhance its inherent ST inhibitory activity.

Among these, the indole alkaloid 3,3′-diindolylmethane (DIM), a metabolic by-product formed during the digestion of cruciferous vegetables, is particularly noteworthy in anticancer research. DIM has been shown to independently suppress metastasis and promote apoptosis across various carcinoma types.[30–32] Moreover, DIM-containing compounds, including naturally occurring derivatives (see Fig. 1) such as vibrindole A,[33] and trisindoline,[34] as well as synthetic analogs like phemindole[35] and SK228,[36,37] exhibit excellent anticancer properties. Inspired by these insights, herein we present the development of LCA-DIM hybrids (depicted in Fig. 1) as a novel class of LCA-based ST inhibitors with enhanced inhibitory activity and selectivity against the *N*-glycan sialylating ST6GAL1, presenting potential as antimetastatic agents against the aggressive triple negative breast cancer (TNBC).

2. Results and discussion

2.1 Design and synthesis of LCA-DIM hybrids

On the design of LCA-based ST inhibitors, most modifications were introduced at the C3–OH region of LCA due to the ST activities of C3–OH modified Lith-O-Asp and AL-10.[21,23] However, recent advancement have introduced modifications at the COOH of LCA to improve the overall ST inhibitory activity and selectivity of LCA-based inhibitors.[24,26]
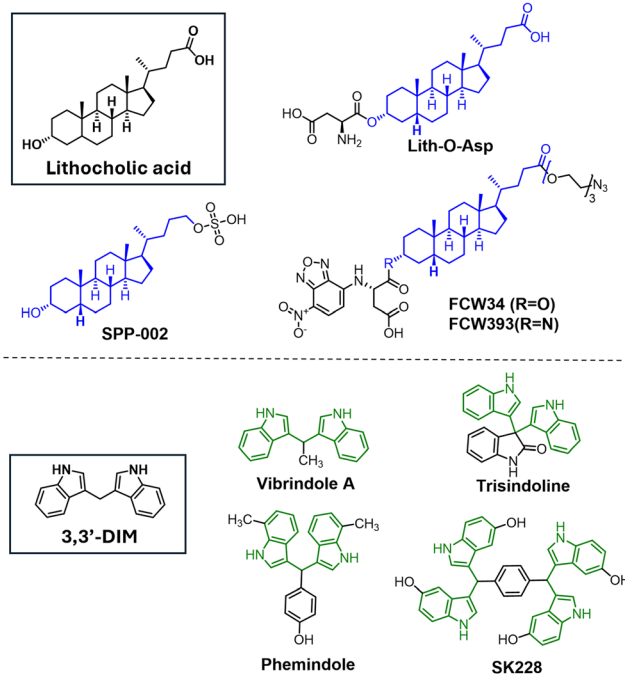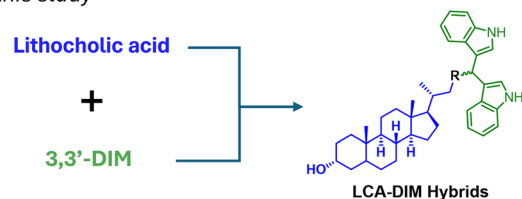

Fig. 1 Structures of representative lithocholic acid (LCA) and 3,3′-diindolylmethane (3,3′-DIM) derivatives, and the schematic representation of the molecular hybridization approach used in this study for the development of LCA-DIM hybrids.

To further utilize this region, we strategically positioned the DIM moiety on the COOH moiety of LCA. For this purpose, we present two LCA-DIM hybrids – the direct LCA-DIM hybrid **4** and the Asp linked LCA-DIM hybrid **11**. The synthetic pathways used for the preparation of the hybrids were detailed in Scheme 1.

Successful synthesis of hybrid **4** was achieved through a four-step synthesis process with an overall yield of 24%. This involved the complete protection of LCA (**1**) through methyl esterification of its COOH group under Fischer conditions, then the silylation of the C3–OH group with *tert*-butyldimethylsilyl chloride (TBSCl) to successfully afford intermediate **2**. Subsequently, the ester group of intermediate **2** was reduced to obtain its alcohol form *via* LAH reduction. The resulting alcohol was then oxidized to its aldehyde form using pyridinium chlorochromate (PCC) as the oxidizing agent, obtaining the LCA-aldehyde intermediate **3** at 50% yield. Finally, the aldehyde intermediate **3** was transformed into LCA-DIM hybrid **4** using 5% I$_2$ in MeOH. In this reaction, the condition simultaneously catalyzes the nucleophilic addition of two indole groups towards
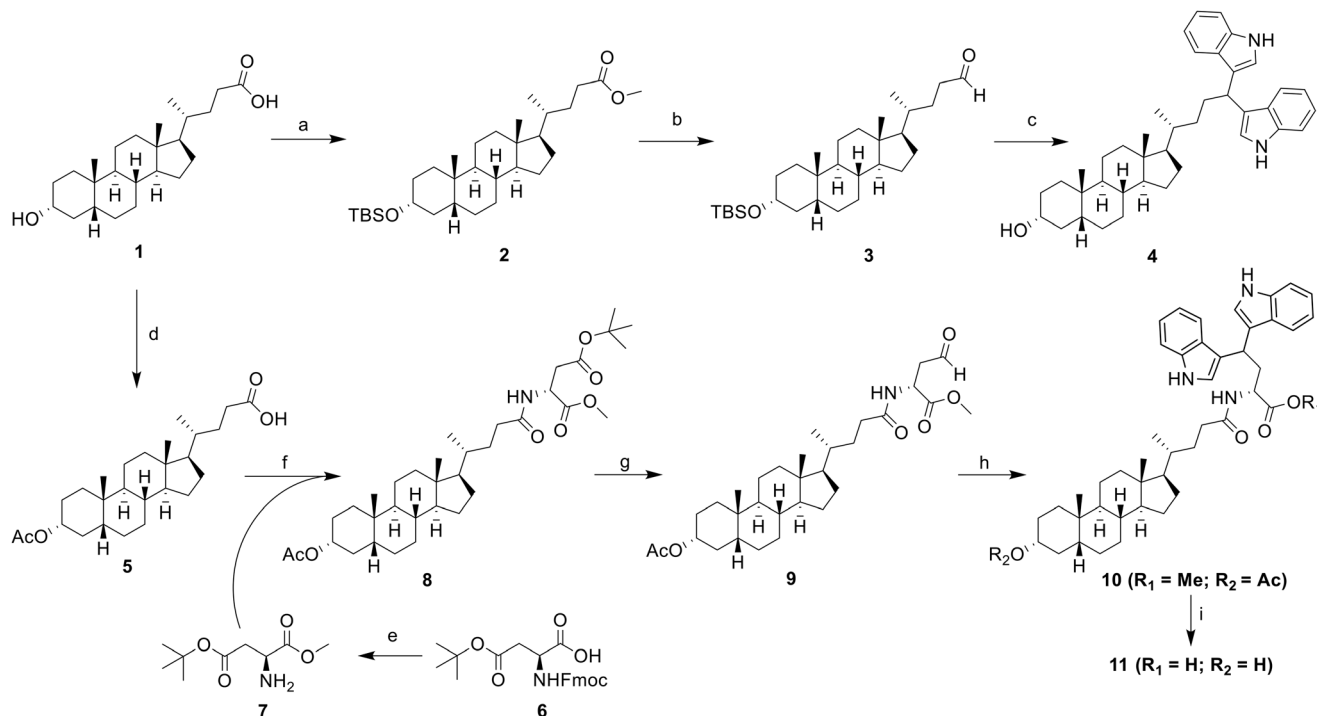
Scheme 1 Synthesis of LCA-DIM hybrids **4** and **11**. Reagents and conditions: a) i) MeOH, cat. HCl, RT, 8 h; ii) TBSCl, imidazole, DMF, 80 °C, 6 h, 64% (over two steps); b) (i) LiAlH$_4$, THF, 0 °C, 4 h; (ii) PCC, DCM, RT, 12 h, 50%; c) indole, 5% I$_2$ in MeOH, RT, 8 h, 41%; d) Ac$_2$O, DMAP, DCM, RT, 2 h, 99%; e) i) EDC, HOBt, TEA, MeOH, DCM, RT, 8 h; ii) 1-dodecanethiol, DBU, DCM, RT, 0.5 h, 97% (over two steps); f) EDC, HOBt, DIPEA, DCM, RT, 8 h, 90%; g) i) TFA, DCM, RT, 2 h; ii) 1-dodecanthiol, EDC, cat. DMAP, DCM, RT, 4 h; iii) Et$_3$SiH, 10% Pd/C, 4 Å MS, THF/acetone, 2–3 h, 55% (over three steps); h) indole, I$_2$, DCM, RT, 88%; i) Ba(OH)$_2$ 8H$_2$O, MeOH, 8 h, RT, 60%.

the intermediate's aldehyde moiety forming the diindolyl motif while removing the silyl ether protection on the hybrid's C3–OH,[38] affording a yield of 41%.

Similar approach was used for the synthesis of the Asp-linked hybrid **11** which involved the preparation of an aldehyde intermediate, followed by I$_2$-catalyzed diindolylation of the aldehyde group forming the DIM motif. Before the preparation of the aldehyde moiety in the structure, the Asp linker was initially introduced in the LCA core. Initially, the C3–OH of LCA was protected through acetylation with acetic anhydride and catalytic amount of DMAP to obtain intermediate **5**. The Asp linker **7** was then synthesized *via* a two-step protection-deprotection process. To begin with, the free COOH group of Fmoc-Asp(O*t*Bu)–COOH (**6**) was coupled with MeOH using EDCI-HCl/HOBt coupling agents and TEA as base. This was followed by Fmoc deprotection, which was carried out using DBU as the deprotection agent and 1-dodecanethiol as the dibenzofulvene scavenging agent to enhance the overall yield of the intermediate. The Asp linker was then introduced on intermediate **5** *via* EDCI-HCl/HOBt/DIPEA-mediated coupling reaction, yielding to the Asp-LCA intermediate **8**. Next step involved the selective reduction of the COO*t*Bu side chain of the Asp-LCA conjugate *via* Fukuyama reduction.[39,40] Initially, the *tert*-butyl protecting group on the linker's side chain was removed with a 1:1 TFA/DCM solvent mixture. The free acid was then coupled with 1-dodecanethiol under Steglich coupling

conditions, and the resulting thioester was subsequently reduced to the aldehyde form *via* Pd-catalyzed reduction, using Et$_3$SiH as the hydride donor. For this reaction, a dry solution of 1:3 acetone/THF was used as solvent and 4 Å molecular sieves were introduced to obtain the LCA-aldehyde **9** with an optimal yield of 55%. The diindolylation of intermediate **9** using I$_2$ as Lewis acid yielded the protected LCA-DIM hybrid **10** at 88% yield. The protected hybrid was then subjected to Ba(OH)$_2$-catalyzed deprotection, simultaneously removing both methyl and acetyl protecting groups. This resulted to the successful synthesis of hybrid **11** at moderate yield of 60%.

2.2 Enhanced ST6GAL1 inhibition and selectivity of LCA-DIM hybrids demonstrating antimigratory properties against MDA-MB-231 cells

The inhibitory effects of the hybrid compounds were assessed against two representative ST isozymes—human α2,6-*N*-sialyltransferase ST6GAL1 and rat α2,3-*O*-sialyltransferase ST3GAL1—using a UPLC-based ST inhibition assay. The results were compared with those of the scaffold LCA and two established LCA-based ST inhibitors, Lith-O-Asp and AL10, as summarized in Table 1. Our findings indicated that the incorporation of the DIM moiety substantially enhanced the ST6GAL1 inhibitory activity of the LCA core, as demonstrated by the ability of hybrid **4** to inhibit the ST's enzymatic activity by

Table 1 Sialyltransferase inhibitory activities of representative LCA-DIM hybrids

| Compound	R	ST6GAL1[a]		ST3GAL1[a]		Selectivity index[b] ($\alpha 2,3$-O/$\alpha 2,6$-N)
		% Inhibition at 25 μM	IC$_{50}$[f] (μM)	% Inhibition at 500 μM	IC$_{50}$[f] (μM)	
4	—	24	—	100	—	—
10	H	61	—	0	—	—
11 (IAN-1B)	H	100	11.3 ± 0.4	3	—	>44
12	NO$_2$	100	—	3	—	—
13 (IAN-5B)	Cl	95	6.6 ± 0.2	0	—	>76
14	F	86	—	1	—	—
15	OMe	84	—	7	—	—
16	OBn	100	—	4	—	—
17	NHBoc	82	—	2	—	—
18 (IAN-15B)	N$_3$	89	3.3 ± 0.1	5	—	>153
LCA[c]	—	0[e]	—	53	—	—
Lith-O-Asp[d]	—	—	15.8 ± 0.1	—	39 ± 1	3
AL10[d]	—	—	1.5 ± 0.5	—	13.2 ± 0.6	9

[a] The selected sialyltransferase (ST) isozymes human $\alpha 2,6$-N-sialyltransferase ST6GAL1 (R&D Systems, catalog #7620-GT) and rat $\alpha 2,3$-O-sialyltransferase ST3GAL1 (Calbiochem, catalog #566227) were used for this study. [b] The selectivity index is defined as the ratio of the calculated IC$_{50}$ for ST3GAL1 (or the highest tested concentration in cases without IC$_{50}$) to the IC$_{50}$ value for ST6GAL1 inhibition without correction. [c] Data obtained from.[26] [d] Data obtained from.[24] [e] Inhibition at 50 μM. [f] The IC$_{50}$ values are presented as mean ± SD from three independent experiments ($n = 3$).

24% at 25 μM, whereas LCA did not exhibit any inhibition, even at 50 μM. Interestingly, hybrid **11** displayed superior ST6GAL1 inhibition, completely suppressing its activity at 25 μM. Its protected counterpart, hybrid **10**, exhibited lower ST6GAL1 inhibition, achieving only 61% inhibition at the same concentration. This suggests that the C3–OH and COOH moieties play a crucial role in the hybrids' ST6GAL1 inhibitory activity. Further analysis of hybrid **11**'s inhibitory activity showed an IC$_{50}$ value of 11.3 ± 0.4 μM against the N-glycan-sialylating ST isozyme, indicating relatively stronger inhibition compared to the C3–OH-modified Lith-O-Asp, which exhibited an IC$_{50}$ of 15.8 ± 0.1 μM. Notably, the Asp-linked hybrids **10** and **11** exhibited minimal inhibition of ST3GAL1—only up to 3% even at 500 μM—while LCA and hybrid **4** showed 53% and 100% inhibition, respectively. In addition to this, hybrid **11** exhibited a significantly higher selectivity index towards ST6GAL1, with an N-to-O selectivity index exceeding 44. This surpasses the selectivity indices of both Lith-O-Asp (N-to-O selectivity index = 3) and AL10 (N-to-O selectivity index = 9), highlighting the apparent selectivity of the extended hybrids towards ST6GAL1.

To further expand the structural diversity and therapeutic potential of this newly discovered ST inhibitor, we prepared a new series of 5,5′-substituted LCA-DIM hybrids **12**–**18** for further biological evaluation. This was inspired by previous studies showing that targeted modifications to the indole rings of DIM-based hybrids can significantly improve their biological activity.[41,42] These hybrids were prepared using the optimized synthetic route used for hybrid **10** and **11**, employing various 5C-substituted indoles (as summarized in Scheme 2) which were obtained at yields ranging from 19% to 74%. Most of the indoles used in this study were commercially available. However, the indoles required for the preparation of hybrids **16** (R = OBn), **17** (R = NHBoc), and **18** (R = N$_3$) were synthesized using the procedure detailed in SI.

Screening of the substituted LCA-DIM hybrids' ST inhibitory activity revealed that most hybrids exhibited robust ST6GAL1 inhibitory activity at 25 μM (≥80% inhibition) and selectivity as shown in Table 1. No clear correlation was observed between the electronic properties of the substituents and the hybrids' ST inhibitory activities, indicating that other factors may drive their intrinsic potency which warrants further investigation.

Given the excellent ST6GAL1 inhibitory activity and selectivity of the LCA-DIM hybrids, we sought to explore their potential as promising therapeutic candidates for targeting cancer. For this purpose, we explored the effect of both LCA-DIM hybrids towards the aggressive, hormonal treatment-resistant triple-negative breast cancer (TNBC), a cancer subtype previously linked to ST6GAL1 overexpression.[10,25,43,44] To assess their efficacy, we evaluated the cytotoxic and anti-migratory effects of the LCA-DIM hybrids on the MDA-MB-231 TNBC cell line using the MTT and transwell migration assays, respectively.
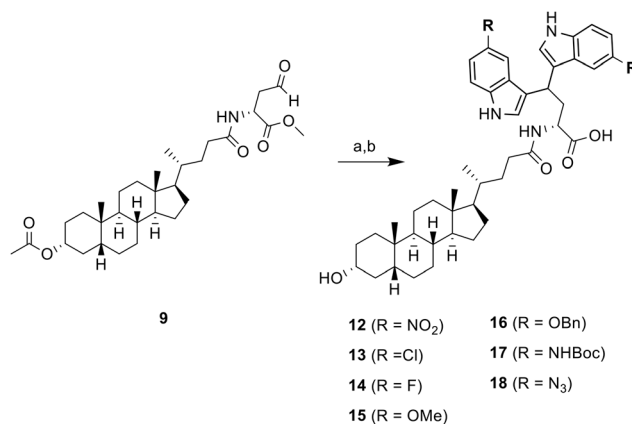
Scheme 2 Synthesis of 5,5′-substituted LCA-DIM hybrids **12**–**18**. a) 5R-indole, I$_2$, DCM/THF, RT, for next step; b) Ba(OH)$_2$ 8H$_2$O, MeOH, 8 h, RT, 19–74%

As shown in Fig. S2, the MTT assay demonstrated that most hybrids exhibited minimal cytotoxicity up to concentrations of 80 μM, except for the halogenated derivatives **13** and **14**. These derivatives showed moderate cytotoxicity, with MTT IC$_{50}$ values ranging from 40 to 80 μM—comparable to that of 3,3′-DIM.

Further investigation with the transwell migration assay revealed that the Asp-linked hybrids **11–18** exhibited observable antimigratory effect at the test concentration of 80 μM (Fig. S3). In contrast, no significant migration inhibition was observed for the direct hybrid **4** or the protected hybrid **10**. The extended hybrids also showed greater antimetastatic potential than 3,3′-DIM, despite presenting cytotoxicity at the tested concentration. Among all the candidates, hybrids **13** (**IAN-5B**, R = Cl) and **18** (**IAN-15B**, R = N$_3$) demonstrated the highest antimetastatic potential against the MDA-MB-231 cell line (Fig. S2). This enhanced activity may be linked to the intrinsic ST6GAL1 inhibitory properties of both hybrids. In the case of **IAN-5B**, its inherent cytotoxicity could also influence its inherent antimigration properties towards the TNBC cell line. Further assessment of the ST inhibitory activity of the hybrids revealed that **IAN-5B** and **IAN-15B** exhibited potent ST6GAL1 inhibition, with IC$_{50}$ values of 6.6 ± 0.2 μM and 3.3 ± 0.1 μM, respectively (Table 1). Additionally, both **IAN-5B** and **IAN-15B** demonstrated enhanced N-to-O selectivity indices (>76 and >153, respectively), significantly surpassing the performance of the unsubstituted hybrid **11** (**IAN-1B**).

2.3 Molecular docking insights into the binding of IAN-5B and IAN-15B towards ST6GAL1

To gain more insights into the excellent ST6GAL1 inhibitory activity of the LCA-DIM hybrids **IAN-5B** and **IAN-15B**, molecular docking studies was conducted using Autodock4. For this study, the ST6GAL1 model used was the crystal structure of human ST6GAL1 (PDB ID: 6QVT).[45] As summarized in Table S1, **IAN-15B** exhibited the strongest binding affinity towards the hST6GAL1 model among the two hybrids, with a binding energy of −10.78 kcal mol^{-1}, while **IAN-5B** showed a slightly lower but comparable binding energy of −10.44 kcal mol^{-1}. These results aligned with the higher experimental ST6GAL1 inhibition observed for **IAN-15B**. Further analysis of the molecular docking results revealed that both hybrids preferentially bind near the enzyme's acceptor site, located between the two polypeptide chains (as illustrated in Fig. S8). This binding motif were consistent with docking results reported for other LCA-based ST inhibitors.[24,46] As shown in Fig. 2, the steroidal core of **IAN-5B** were involved in multiple hydrophobic interactions with several amino acid residues of hST6GAL1 including PRO259(A), VAL261(A), PRO320(A), TRP302(A), as well as their counterparts PRO259(B), VAL261(B), and PRO320(B). Moreover, the carboxyl group of **IAN-5B's** Asp linker formed key hydrogen bonds with GLN235(B) and LYS268(A), underscoring the importance of this functional group in binding towards ST6GAL1. The chloro-
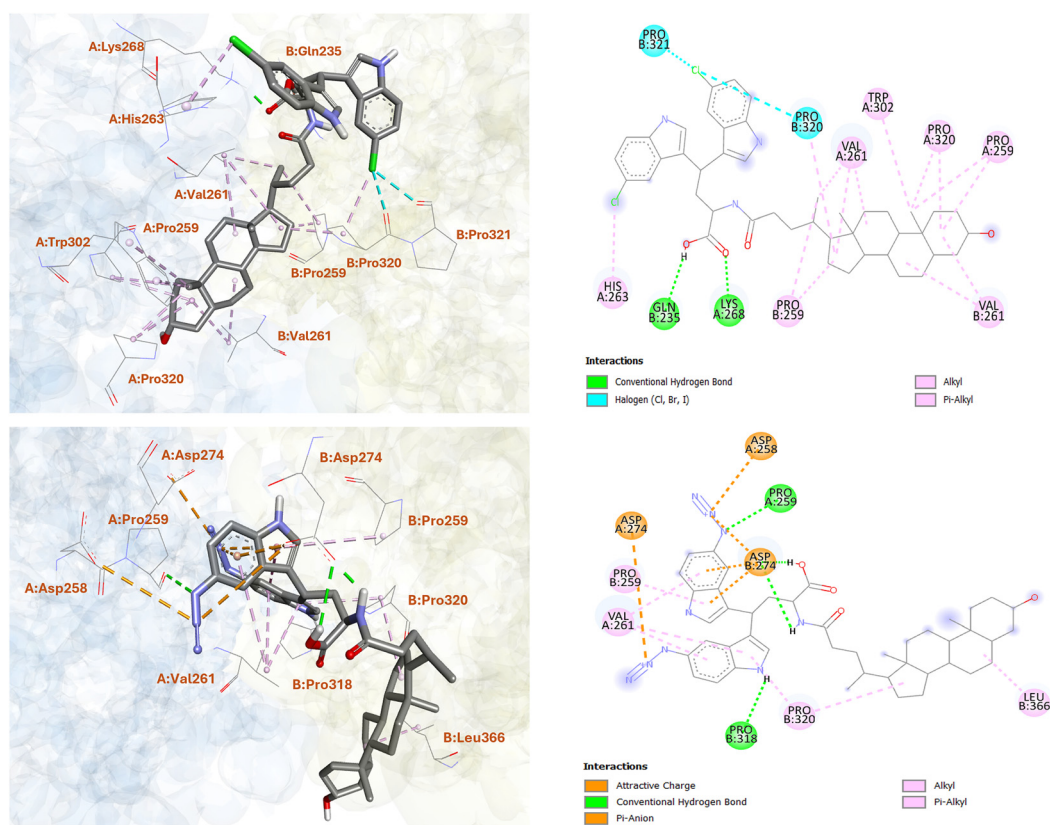

Fig. 2 Molecular docking analysis of LCA-DIM hybrids **IAN-5B** (upper) and **IAN-15B** (lower) with the hST6GAL1 model. The two- and three-dimensional representations illustrate the binding orientation and key interactions of the hybrids within the active site of hST6GAL1.

substituted DIM moiety also shown contribution to the overall interaction of the hybrid towards hST6GAL1, establishing hydrophobic and polar halogen interactions with HIS263(A), PRO320(B), and PRO321(B) as shown in Fig. 2.

On the other hand, the azido-substituted **IAN-15B**, showed fewer interaction with its steroidal ring structure, forming hydrophobic contacts primarily with PRO320(B) and LEU366(B). However, it exhibited enhanced interactions through its DIM and Asp-linker moieties. For instance, the carboxyl and amide NH groups of the Asp-linker form strong hydrogen bonds with ASP274(B) (as shown in Fig. 2), while the azido groups of the DIM moiety participate in electrostatic interactions with ASP258(A) and ASP274(A), and hydrogen bonding with PRO259(A). Additional π-alkyl and π-anion interactions were also observed between the indole ring of **IAN-15B** and residues PRO259(B), VAL261(A), and ASP274(B), respectively. Remarkably, these observed binding patterns of the LCA-DIM hybrids toward hST6GAL1 model were particularly significant given that X-ray crystallography studies have highlighted the role of residue PRO320 in stabilizing HIS370, a critical catalytic residue of ST6GAL1.[47] Furthermore, ASP274 has been shown to play a crucial role in mediating interactions with the donor substrate

CMP-Neu5Ac during the sialylation process. The strong interactions formed by both **IAN-5B** and **IAN-15B**—especially through their DIM-Asp linker regions—with PRO320, ASP274, and adjacent residues, likely disrupt the proper structural alignment and catalytic function of HIS370, thereby impairing ST6GAL1 enzymatic activity. In addition to these, it should be noted that C3–OH group of both **IAN-5B** and **IAN-15B** did not engage in any interactions with the surrounding amino acid residues of ST6GAL1. This lack of involvement suggests that the C3–OH position could be further structurally modified, offering an opportunity to further enhance the potency and overall efficacy of these ST inhibitors. In total, these findings offer valuable insights into the underlying mechanism of inhibition and emphasize the critical role of the DIM moiety in enhancing the overall ST6GAL1 inhibitory activity of the LCA-DIM hybrids.

2.4 Further biological evaluation of IAN-5B and IAN-15B towards various TNBC and HUVEC cell lines

We further explored their antimigratory properties and cytotoxicity towards MDA-MB-231 cells and two additional TNBC cell lines - BT549 and Hs578T. Initially, the cytotoxicity
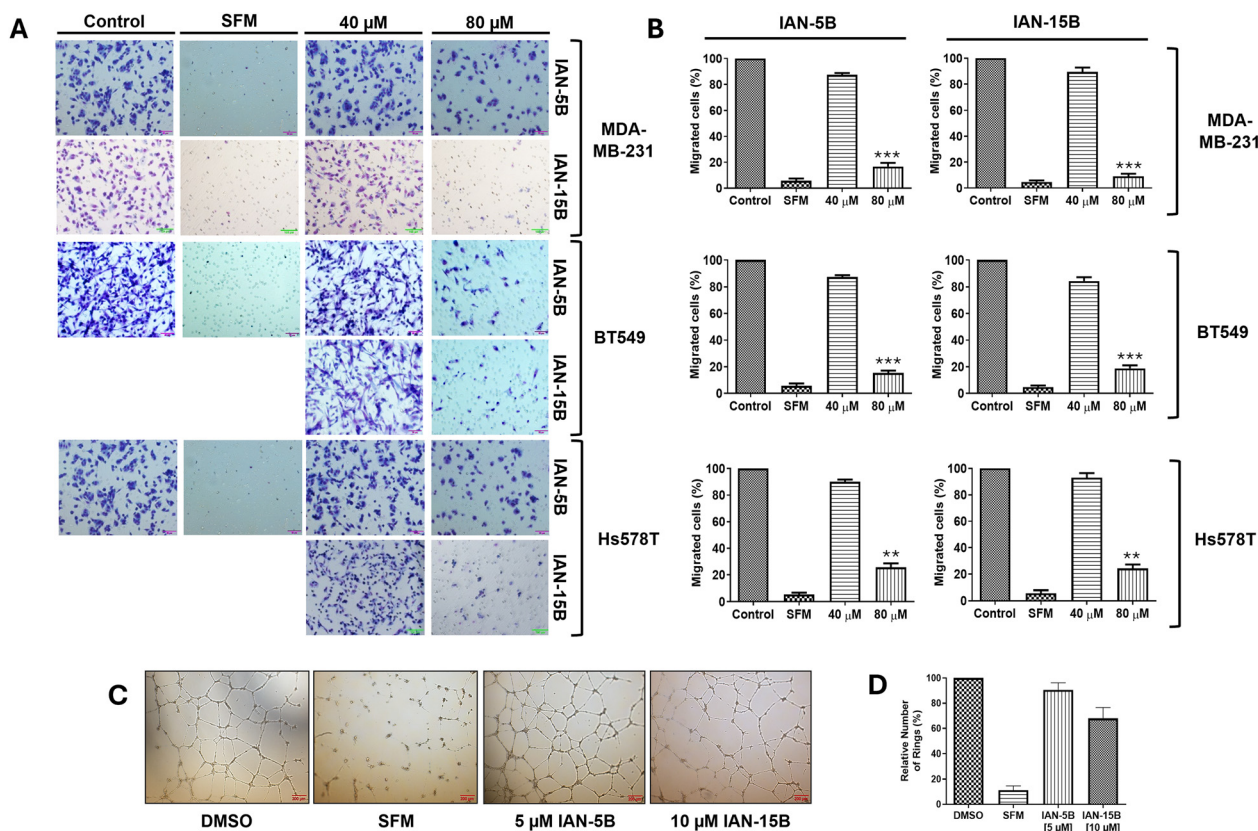
Fig. 3 Evaluation of the antimigratory and antiangiogenic effects of **IAN-5B** and **IAN-15B**. (A) Representative images of the inhibitory effects of **IAN-5B** and **IAN-15B** on the migration of triple-negative breast cancer (TNBC) cell lines BT549, Hs578T, and MDA-MB-231 following 16 hours of incubation with varying concentrations (0, 40, and 80 μM). DMSO and serum-free medium (SFM) were used as control for this study. Several experimental runs were performed using the same control. (B) Quantification of transwell migration assay data against BT549, Hs578T, and MDA-MB-231 TNBC cell lines performed in triplicates. (C) Evaluation of HUVEC tube formation in the presence of non-cytotoxic concentrations of **IAN-5B** (5 μM) and **IAN-15B** (10 μM), with DMSO and serum-free medium serving as controls. (D) Quantification of HUVEC tube formation assay performed in triplicates. All data are presented as mean ± SEM from three independent experiments (*: $p < 0.05$, **: $p < 0.01$, ***: $p < 0.001$).
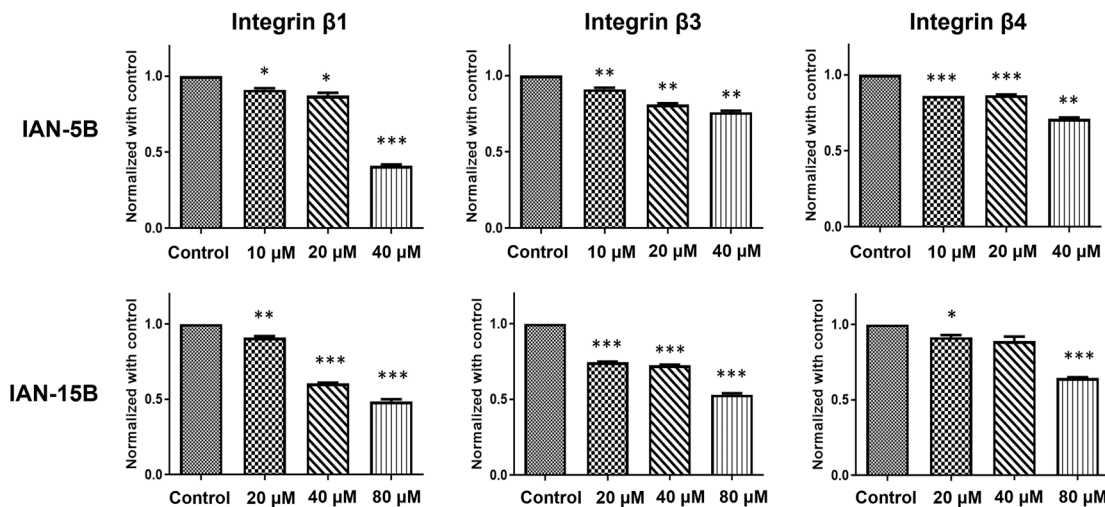
Fig. 4 Influence of LCA-DIM hybrids towards integrin sialylation. Lectin affinity assays followed by western blot analysis revealed a concentration-dependent reduction in $\alpha 2,6$-sialylated integrin subunits $\beta 1$, $\beta 3$, and $\beta 4$ upon treatment with **IAN-5B** and **IAN-15B**. MDA-MB-231 cells were treated with **IAN-5B** at 10, 20, and 40 μM, and with **IAN-15B** at 20, 40, and 80 μM. All data are presented as mean $\pm$ SEM from three independent experiments (*: $p < 0.05$, **: $p < 0.01$, ***: $p < 0.001$).

of the LCA-DIM hybrids was tested against the two additional cell lines *via* MTT assay. Consistent with their effects on the MDA-MB-231 cell line, both hybrids exhibited comparable cytotoxic activities against BT549 and Hs578T with MTT IC$_{50}$ values between 40–80 μM (Fig. S7). Afterwards, the effect of **IAN-5B** and **IAN-15B** on cancer cell migration were tested in all three TNBC cell lines using transwell migration assay at the 40 and 80 μM test concentrations. As illustrated in Fig. 3, both hybrids effectively suppressed cell motility across the three TNBC cell lines, resulting in up to a 10% reduction in cancer cell migration at 80 μM, with migration IC$_{50}$ values ranging from 40–80 μM. The effect of both hybrids on tumorigenic angiogenesis was also assessed *via* HUVEC tube formation assay. Results showed that both hybrids **IAN-5B** and **IAN-15B** presented high cytotoxicity towards HUVEC (Fig. S7), with MTT IC$_{50}$ values of approximately 10 μM and 10–20 μM, respectively. Furthermore, both hybrids inhibited tube formation in HUVEC cells at non-cytotoxic concentrations, with **IAN-15B** showing the strongest anti-angiogenic effect—reducing tube formation to 67% relative to the control at a 10 μM test concentration.

Given the strong antimigratory effects of **IAN-5B** and **IAN-15B**, we aimed to investigate the underlying mechanisms further. We suspect that the inherent antimigratory properties of the LCA-DIM hybrids may be attributed to their impact on the sialylation of cancer cells which contributes to its progression. Prior studies have demonstrated integrin sialylation as a key factor in cancer cell migration and metastasis and the ability of ST inhibitors to target this biological pathway.[3,25,46,48] Based on these findings, we propose that the strong ST6GAL1 inhibitory activity of **IAN-5B** and **IAN-15B** may effectively suppress integrin sialylation, thereby impeding cancer cell motility. To investigate the involvement of both LCA-DIM hybrids towards this mechanism, lectin affinity assays were conducted using the $\alpha 2,6$-sialylation-specific

Sambucus nigra agglutinin (SNA) lectin, followed by western blotting to detect integrin subunits $\beta 1$, $\beta 3$, and $\beta 4$ in MDA-MB-231 cells. Remarkably, both hybrids decreased the levels of captured sialylated integrins, in a dose-dependent manner even at non-toxic concentrations, as shown in Fig. 4. The effects of both hybrids were especially prominent on the $\beta 1$ integrin subunit, which is strongly associated with ST6GAL1-mediated sialylation and has been closely linked to cancer progression.[49–51] Overall, these findings highlight the potential antimetastatic and antiangiogenetic potential of LCA-DIM hybrids, offering a promising foundation for further exploration of their therapeutic potential in cancer treatment.

3. Conclusion

In response to the growing demand for compounds capable of inhibiting ST activity as potential therapeutic strategy, this study employed molecular hybridization for the development of the novel LCA-DIM hybrids as potential ST inhibitors. These hybrids presented heightened inhibitory activity and apparent selectivity towards ST6GAL1, with the introduction of an Asp linker between the LCA and DIM moiety further enhanced the hybrids' ST6GAL1 activity. Molecular docking data also supports these findings, indicating the significance of the hybrids' DIM moiety and Asp linker on its binding towards the ST6GAL1 model. Cell-based assays have also revealed that most of the hybrids have low cytotoxicity profiles in exception for the halogen-substituted series. Moreover, the hybrids demonstrate excellent antimigration effects with **IAN-5B** and **IAN-15B** demonstrating the highest antimetastatic potential against three TNBC cell lines (MDA-MB-231, BT549, and Hs578T), correlating to their enhanced ST6GAL1 inhibitory activities (IC$_{50}$ = 6.6 $\pm$ 0.2 and 3.3 $\pm$ 0.1, respectively). In addition to this, **IAN-15B** presented antiangiogenetic effect towards HUVEC as presented in the

tube formation assay data. We have also revealed the involvement of both hybrids in reducing β integrin sialylation, which could be attributed to its inherent anticancer properties. In summary, this study introduced the LCA-DIM hybrid as a novel and potent ST inhibitor, highlighting the potential of molecular hybridization for the development of targeted therapies for the aggressive TNBC with promising *N*-glycan selectivity.

4. Experimental section

4.1 Chemistry

4.1.1 General remarks. Reagents for this study were commercially purchased and used without any further purification. All solvents were anhydrous grade unless indicated otherwise. Reactions were monitored *via* thin layer chromatography (TLC) *via* silica gel 60 F_{254} (Merck) and purification *via* column chromatography were performed with silica gel 60 (230–400 mesh) (Merck). ^{1}H NMR and ^{13}C NMR spectra were recorded with either Bruker AVIII-400, AV-400, or AV-500 from the Institute of Chemistry, Academia Sinica. Chemical shifts were reported in parts per million (ppm) relative to the residual deuterated solvent used (d_1-chloroform 1H = 7.26 ppm, ^{13}C = 77.0 ppm; d_6-acetone ^{1}H = 2.05 ppm, ^{13}C = 29.84 ppm; 206.26 ppm). Multiplicities are reported using the following abbreviations: s = singlet, d = doublet, t = triplet, q = quartet, m = multiplet, dd = double doublet, J = coupling constant values in Hertz. Mass spectra were analyzed by JMS-T100LP AccuTOF LC-plus 4G TOF mass spectrometer (JEOL, Tokyo, Japan). Purity of compounds were established as >95% using reversed-phase HPLC (stationary phase and conditions are listed in the SI).

4.1.2 Synthesis of direct LCA-DIM hybrid

4.1.2.1. Synthesis of intermediate 2. Lithocholic acid (1) (10 g, 1.0 eq.) was added to a stirring solution of MeOH. After a few minutes, 5 drops of H_2SO_4 were introduced to the mixture. The reaction was stirred overnight, after which it was neutralized using saturated $NaHCO_3$ solution to quench the reaction. The resulting precipitate was filtered, collected, and dried to yield OMe-protected LCA as a white solid. Afterwards, 1.5 g (1.0 eq.) of the protected LCA was dissolved in DMF together with 0.87 g (1.5 eq.) of *tert*-butyldimethylsilyl chloride and 0.52 g (2.0 eq) of imidazole. The reaction mixture was heated to 60 °C and was allowed to react for 8 h. Upon completion, the reaction was quenched with ethyl acetate, and the organic layer was extracted with distilled H_2O three times to remove most of the DMF and was washed with brine. The resulting solution was then dried over $MgSO_4$, and the solvent was removed under reduced pressure to obtain intermediate 2 as a white powder which was used without further purification. Yield: 64% (1.25 g, for two steps). ^{1}**H NMR** (400 MHz, CDCl$_3$): δ (ppm) 3.67 (s, 3H), 3.63–3.52 (m, 1H), 2.42–2.32 (m, 1H), 2.29–2.15 (m, 1H), 1.98–1.92 (m, 1H), 1.90–1.71 (m, 5H), 1.65–1.52 (m, 2H), 1.46–1.31 (m, 9H), 1.30–1.20 (m, 3H), 1.20–0.96 (m, 5H), 0.95–0.87 (m, 16H), 0.65 (s, 3H). ^{13}**C NMR** (100 MHz, CDCl$_3$): δ (ppm) 174.8, 72.9, 56.5, 56.0, 51.5, 42.8, 42.4, 40.3, 40.2, 37.0, 35.9, 35.6, 35.4, 34.6,

31.1 (3C), 28.2, 27.4, 26.4, 26.0 (3C), 24.3, 23.4, 20.9, 18.4, 18.3, 12.1, −4.5 (2C).

4.1.2.2. Synthesis of intermediate 3. In a dry round-bottom flask, 1.75 g (1.0 eq.) of intermediate 2 was dissolved in anhydrous THF and stirred at 0 °C. After a few minutes, 0.53 g (5.0 eq.) of LiAlH$_4$ was added to the cooled solution, and the reaction was allowed warm to room temperature and was stirred for 3 h. For work-up, saturated Rochelle salt solution was slowly added to the reaction mixture until the vigorous reaction ceased. Additional amounts of Rochelle salt solution and ethyl acetate were then added, and the mixture was stirred overnight. The organic layer was subsequently washed with distilled water and brine, then dried under vacuum to yield the reduced LCA intermediate as a white solid. The obtained solid was dissolved in DCM, and 1.66 g (2.0 eq.) of pyridinium chlorochromate was added to the solution. After stirring for 12 h, the reaction mixture was filtered through celite. The filtrate was washed with distilled H_2O and brine, dried over MgSO$_4$, and concentrated to afford the crude product. The crude product was purified by flash chromatography using ethyl acetate/hexane solvent system to yield intermediate 3 as a white crystalline solid. Yield: 50% (0.82 g). ^{1}**H NMR** (400 MHz, CDCl$_3$): δ (ppm) 9.72 (s, 1H), 3.60–3.50 (m, 1H), 2.48–2.20 (m, 2H), 1.93–1.70 (m, 6H), 1.58–1.48 (m, 2H), 1.41–1.31 (m, 7H), 1.29–1.19 (m, 4H), 1.18–1.11 (m, 2H), 1.08–0.95 (m, 4H), 0.91–0.82 (m, 16H), 0.61 (s, 3H), 0.02 (s, 6H). ^{13}**C NMR** (100 MHz, CDCl$_3$): δ (ppm) 202.9, 72.8, 56.4, 56.0, 42.7, 42.3, 40.9, 40.3, 40.2, 36.9, 35.9, 35.6, 35.3, 34.6 (2C), 31.0, 28.2, 28.0, 26.4, 26.0 (3C), 24.2, 23.4, 20.8, 18.4, 18.3, 12.0, −4.6 (2C).

4.1.2.3. Synthesis of LCA-DIM hybrid 4. Intermediate 3 (0.4 g, 1.0 eq.) was dissolved in 5% I$_2$ in MeOH, followed by the addition of 0.30 g (3.0 eq.) of indole. The reaction mixture was stirred for 6 h, then dried and diluted with ethyl acetate. The organic layer was sequentially washed with Na$_2$S$_2$O$_3$, distilled H$_2$O and brine. It was then dried over MgSO$_4$ and concentrated to yield the crude product. The crude was then purified using flash chromatography using ethyl acetate/hexane solvent system to obtain hybrid 4 as brown solid. Yield: 41% (0.20 g). ^{1}**H NMR** (400 MHz, CDCl$_3$): δ (ppm) 7.97 (br s, 1H), 7.93 (br s, 1H), 7.69–7.60 (m, 2H), 7.34–7.27 (m, 2H), 7.16 (t, J = 7.3 Hz, 2H), 7.07 (d, J = 7.3 Hz, 2H), 6.94 (s, 1H), 6.90 (s, 1H), 4.43 (t, J = 7.3 Hz, 1H), 3.70–3.60 (m, 1H), 2.35–2.25 (m, 1H), 2.21–2.10 (m, 2H), 2.02–1.95 (m, 1H), 1.90–1.78 (m, 3H), 1.78–1.68 (m,2H), 1.62–1.51 (m, 3H), 1.1.46–1.38 (m, 6H), 1.33–1.20 (m, 3H), 1.17–1.08 (m, 4H), 1.03–0.95 (m, 8H), 0.64 (s, 3H). ^{13}**C NMR** (100 MHz, CDCl$_3$): δ (ppm) 136.6 (2C), 127.2, 127.1, 121.6 (2C), 121.5, 121.3, 120.8, 120.3, 119.6, 119.5, 118.9 (2C), 111.1 (2C), 71.9, 56.4, 56.0, 42.6, 42.1, 40.4, 40.1, 36.4, 35.8 (2C), 35.3, 34.6, 34.5, 34.4, 32.3, 30.5, 28.2, 27.2, 26.4, 24.2, 23.4, 20.8, 18.8, 12.0. **HRMS (ESI)** calculated for C$_{40}$H$_{51}$N$_2$O (M − H)$^-$, 575.4007; found, 575.3999. HPLC purity: >99%.

4.1.3 Synthesis of Asp linked LCA-DIM hybrid

4.1.3.1. Synthesis of intermediate 5. Lithocholic acid (1) (10 g, 1.0 eq.) was placed in a dry round bottom flask along with approximately 20 mL (4.0 eq.) of acetic anhydride and a catalytic amount of DMAP (0.05 eq.) in DCM. The mixture

was stirred at room temperature for 2 h. The reaction was then quenched with $NaHCO_3$, and the organic layer was then washed with saturated $NaHCO_3$ solution, distilled H_2O, and brine. After drying over $MgSO_4$, the solvent was evaporated under reduced pressure to yield intermediate **5** as a white powder solid. Yield: ≥ 99% (11 g). **¹H NMR** (400 MHz, CDCl₃): δ (ppm) 10.43 (br, 1H), 4.71–4.61 (m, 1H), 2.39–2.15 (m, 2H), 1.97 (s, 3H), 1.94–1.88 (m, 1H), 1.85–1.71 (m, 5H), 1.67–1.60 (m, 1H), 1.56–1.45 (m, 2H), 1.44–1.27 (m, 8H), 1.23–1.13 (m, 3H), 1.12–0.92 (m, 6H), 0.90–0.84 (m, 6H), 0.60 (s, 3H); **¹³C NMR** (100 MHz, CDCl₃): δ (ppm) 180.3, 170.8, 74.4, 56.5, 56.0, 42.7, 41.9, 40.4, 40.1, 35.8, 35.3, 35.0, 34.5, 32.2, 31.0, 30.8, 28.2, 27.0, 26.6, 26.3, 24.2, 23.3, 21.4, 20.8, 18.2, 12.0.

4.1.3.2. Synthesis of intermediate 7. To a stirring solution of DCM, 10.0 g (1.0 eq.) of Fmoc-Asp(O*t*Bu)–COOH (**6**) were added together with EDCI-HCl (4.7 g, 1.0 eq.), HOBt (4.1 g, 1.1 eq.), TEA (~3.5 mL, 1.0 eq.), and 1 mL of MeOH. The mixture was stirred for 8 h, and upon completion, the reaction was diluted with DCM and quenched with dilute HCl. The precipitates were removed *via* filtration, and the organic layer was sequentially washed with dilute HCl, $NaHCO_3$, distilled H_2O, and brine. The organic phase was dried over $MgSO_4$, and the solvent was evaporated under reduced pressure, yielding the fully protected acid as a white crystalline solid. The solid was then dissolved in DCM, and approximately 7.4 g DBU (3.0 eq) was added to the stirring solution alongside 15 mL of 1-dodecanethiol was introduced, and the reaction mixture was stirred for 30 minutes. The solvent was subsequently removed under reduced pressure, and the resulting slurry was immediately purified *via* flash chromatography using ethyl acetate and hexane solvent system to afford intermediate **7** as a clear yellow liquid. Yield: 97% (4.6 g). **¹H NMR** (400 MHz, CDCl₃): δ (ppm) 3.58–3.52 (m, 4H), 2.54–2.44 (m, 2H), 1.67 (s, 2H), 1.25 (s, 9H); **¹³C NMR** (100 MHz, CDCl₃): δ (ppm) 174.5, 170.0, 80.7, 51.8, 51.0, 39.9, 27.7 (3C).

4.1.3.3. Synthesis of intermediate 8. In a round-bottom flask, approximately 2.0 g of intermediate **5** (1.0 eq.) and 1.8 g of intermediate **7** (1.5 eq.) were dissolved in DCM. The solution was stirred for a few minutes before adding EDCI-HCl (1.9 g, 1.1 eq.), HOBt (1.5 g, 1.1 eq.), and DIPEA (~1.5 mL, 1.0 eq.). The reaction mixture was stirred for 8 h, and upon completion, it was diluted with DCM. The organic layer was washed sequentially with dilute HCl, saturated $NaHCO_3$, and brine. After drying over $MgSO_4$, the solvent was removed under reduced pressure to yield the crude product. This was subsequently purified by flash chromatography with solvent system of ethyl acetate and hexane to afford the conjugate **8** as a white foamy solid. Yield: 90% (4.0 g). **¹H NMR** (400 MHz, CDCl₃): δ (ppm) 6.59 (d, J = 7.98 Hz, 1H), 4.72–4.51 (m, 2H), 3.59 (s, 3H), 2.73 (dd, J = 16.7, 4.6 Hz, 1H), 2.59 (dd, J = 16.7, 4.5 Hz, 1H), 2.22–2.09 (m, 1H), 2.06–1.93 (m, 1H), 1.91–1.80 (m, 4H), 1.75–1.62 (m, 5H), 1.58–1.50 (m, 1H), 1.46–1.36 (m, 2H), 1.33–1.22 (m, 16H), 1.16–1.06 (m, 4H), 0.99–0.87 (m, 5H), 0.85–0.75 (m, 7H), 0.51 (s, 3H); **¹³C NMR** (100 MHz,

CDCl₃): δ (ppm) 173.1, 171.2, 170.2, 169.9, 81.2, 74.1, 56.3, 55.9, 52.2, 48.4, 42.5, 41.7, 40.2, 39.9, 37.3, 35.6, 35.2, 34.8, 34.3, 33.0, 32.0, 31.4, 27.9, 27.7 (3C), 26.8, 26.4, 26.1, 24.0, 23.1, 21.1, 20.6, 18.1, 11.8.

4.1.3.4. Synthesis of intermediate 9. Intermediate **8** (2.4 g, 1.0 eq.) was dissolved in a 1:1 TFA/DCM solution in a round-bottom flask and allowed to react for 2 h. The reaction mixture was then concentrated using a rotary evaporator to yield the free acid intermediate, which was used directly in the next step without further purification. The deprotected precursor was dissolved in DCM, and 1.4 g of EDCI-HCl (1.5 eq.), 3 mL of 1-dodecanethiol (~3.0 eq), and 0.024 g of DMAP (0.05 eq.) were added. The mixture was stirred for 4 h, after which the solution was dried under reduced pressure. Excess 1-dodecanethiol was removed by flash chromatography to obtain the thioester precursor as a white crystalline solid. Afterwards, 1 g of the precursor was then dissolved in a 1:1 mixture of THF/acetone with 4 Å molecular sieves. A catalytic amount of 10% Pd/C (100 mg, 5% w/w) was added, and the system was purged with argon gas to maintain an inert atmosphere. After a few minutes, 3.0 eq. of Et₃SiH (0.68 mL) were added. Once the effervescence ceased, the reaction mixture was filtered through celite, and the filtrate was concentrated using a rotary evaporator. The crude product was purified by flash chromatography using ethyl acetate and hexane solvent system to yield the desired product **9** as a white solid. Yield: 55% (0.53 g), for three steps. **¹H NMR** (400 MHz, CDCl₃): δ (ppm) 9.68 (s, 1H), 6.45 (d, J = 7.7 Hz, 1H), 4.85–4.62 (m, 2H), 3.71 (s, 3H), 3.14–2.98 (m, 2H), 2.26–2.18 (m, 1H), 2.13–2.05 (m, 1H), 1.99 (s, 3H), 1.95–1.90 (m, 1H), 1.86–1.72 (m, 5H), 1.68–1.60 (m, 1H), 1.56–1.47 (m, 2H), 1.44–1.30 (m, 7H), 1.27–1.18 (m, 4H), 1.13–0.94 (m, 6H), 0.90–0.85 (m, 6H), 0.60 (s, 3H); **¹³C NMR** (100 MHz, CDCl₃): δ (ppm) 199.6, 173.5, 171.3, 170.7, 74.5, 56.5, 56.1, 52.9, 47.2, 45.7, 42.8, 41.9, 40.5, 40.2, 35.8, 35.5, 35.1, 34.6, 33.3, 32.3, 31.5, 28.3, 27.1, 26.7, 26.4, 24.2, 23.4, 21.5, 20.9, 18.4, 12.1.

4.1.3.5. Synthesis of protected Asp-linked LCA-DIM hybrids 10. In a round bottom flask, 0.30 g of aldehyde intermediate **9** (1.0 eq.) was dissolved in THF along with 0.20 g (3.0 eq.) of indole. After a few minutes of stirring, catalytic amount of I₂ (0.045 g, 0.05 eq.) was added into the solution and the reaction was monitored *via* TLC. Upon completion, the reaction mixture was concentrated, and ethyl acetate was added, and the resulting solution was washed with $Na_2S_2O_3$, distilled H_2O, and brine. The organic layer was dried over $MgSO_4$ and concentrated *in vacuo*. The obtained crude product was purified *via* flash chromatography using ethyl acetate and hexane solvent system to obtain the protected hybrid **10**. Obtained as off-white powder. Yield: 88% (0.32 mg). **¹H NMR** (500 MHz, CDCl₃): δ (ppm) 8.29 (s, 2H), 7.54 (d, J = 7.9 Hz, 1H), 7.51 (d, J =7.9 Hz, 1H), 7.26 (d, J = 2.1 Hz, 1H), 7.25 (d, J = 2.1 Hz, 1H), 7.12 (t, J = 7.5 Hz, 2H), 6.87–7.05 (m, 4H), 5.98 (d, J = 7.5 Hz, 1H), 4.70–4.76 (m, 2H), 4.56 (t, J = 7.4 Hz, 1H), 3.51 (s, 3H), 2.58–2.81 (m, 2H), 1.96–2.05 (m, 4H), 1.91–1.95 (m, 1H), 1.75–1.89 (m, 5H), 1.60–1.72 (m, 2H), 1.51–1.57 (m, 2H), 1.32–1.47 (m, 7H), 1.17–1.27(m, 4H), 0.99–

1.15 (m, 6H), 0.81–0.93 (m, 6H), 0.6 (s, 3H); ^{13}C NMR (125 MHz, CDCl$_3$): δ (ppm) 173.7, 173.2, 170.9, 136.8, 136.7, 126.7, 126.5, 122.5, 122.2, 121.9, 121.9, 119.5, 119.4, 119.3, 119.2, 118.3, 118.1, 111.5, 111.4, 74.6, 56.5, 56.0, 52.2, 51.8, 42.8, 42.0, 40.5, 40.2, 37.4, 35.9, 35.5, 35.1, 34.7, 33.3, 32.4, 31.6, 31.2, 28.3, 27.1, 26.7, 26.4, 24.3, 23.4, 21.6, 20.9, 18.4, 12.1; **HRMS** (ESI) calculated for C$_{47}$H$_{61}$N$_3$O$_5$Na (M + Na)$^+$, 770.4503; found, 770.4509. HPLC purity: 97%.

4.1.3.6. Synthesis of Asp-linked hybrid 11. For deprotection, the purified intermediate **10** was dissolved in methanol (MeOH) in a round-bottom flask and Ba(OH)$_2$·8H$_2$O (3.0 eq) was added to the solution. The reaction mixture was allowed to react for 8 h and upon completion, the solution was diluted with ethyl acetate and sequentially washed with dilute HCl and brine. The organic layer was dried over MgSO$_4$ and concentrated using rotary evaporator. The crude product was then recrystallized to obtain the LCA-DIM hybrid **11**. Obtained as brown solid. Yield: 60% (0.15 g). ^{1}H NMR (500 MHz, acetone-d_6): δ (ppm) 10.08 (br s, 1H), 10.02 (br s, 1H), 7.56 (t, J = 9.0 Hz, 2H), 7.49 (d, J = 7.9 Hz, 1H), 7.40–7.20 (m, 4H), 7.05–6.85 (m, 4H), 4.73 (q, J = 5.0 Hz, 1H), 4.55–4.50 (m, 1H), 3.60–3.48 (m, 1H), 2.92–2.80 (m, 1H), 2.65–2.55 (m, 1H), 2.80–2.35 (m, 2H), 1.99–1.93 (m, 1H), 1.92–1.73 (m, 5H), 1.64–1.52 (m, 2H), 1.50–1.32 (m, 8H), 1.32–1.13 (m, 6H), 1.13–0.98 (m, 3H), 0.97–0.89 (m, 7H), 0.65 (s, 3H); ^{13}C NMR (125 MHz, acetone-d_6): δ (ppm) 174.7, 174.5, 138.1, 137.9, 127.9, 127.7, 123.6, 122.7, 121.8, 121.8, 120.2, 120.1, 119.6, 119.1, 119.0, 118.2, 112.2, 112.0, 79.1, 71.7, 57.2, 56.8, 52.2, 43.4, 42.9, 41.2, 40.9, 38.2, 37.2, 36.6, 36.2, 35.2, 33.4, 32.6, 31.9, 31.2, 28.9, 28.0, 27.2, 24.9, 23.9, 21.5, 18.8, 12.4; **HRMS** (ESI) calculated for C$_{44}$H$_{57}$N$_3$O$_4$Na (M + Na)$^+$, 714.4241; found, 714.4251. HPLC purity: >99%.

4.1.3.7. Synthesis of Asp-linked hybrid 12. Prepared following the general diindolylation and deprotection procedure previously described for hybrids **10** and **11** using 5-nitro-1H-indole. Obtained as bright yellow solid. Yield: 47% (0.35 g, for two steps). ^{1}H NMR (500 MHz, acetone-d_6): δ (ppm) 11.01 (s, 1H), 10.95 (s, 1H), 7.49–8.59 (m, 9H), 4.91 (q, J = 4.8 Hz, 1H), 4.54–4.67 (m, 2H), 3.50–3.58 (s, 1H), 2.90–2.98 (m, 1H), 2.68–2.78 (m, 1H), 2.16–2.42 (m, 2H), 1.86–1.94 (m, 1H), 1.70–1.85 (m, 5H), 1.58–1.64 (m, 1H), 1.39–1.48 (m, 3H), 1.16–1.38 (m, 10H), 0.92–1.15 (m, 6H), 0.85–0.92 (m, 7H), 0.57 (s, 3H); ^{13}C **NMR** (125 MHz, acetone-d_6): δ (ppm) 175.0, 174.3, 141.7 (2C), 141.1, 141.0, 127.7, 127.0, 126.7 (2C), 121.6, 120.1, 117.6, 117.5, 116.9, 116.9, 112.7, 112.6, 71.7, 57.2, 56.8, 51.8, 43.3, 42.9, 41.2, 40.9, 38.0, 37.2, 36.6, 36.2, 35.2, 35.2, 33.5, 32.6, 31.5, 31.2, 28.8, 27.9, 27.1, 24.7, 24.7, 23.8, 21.4, 18.8, 12.3; **HRMS** (ESI) calculated for C$_{44}$H$_{55}$N$_5$O$_8$Na (M + Na)$^+$, 804.3943; found, 804.3950. HPLC purity: >99%.

4.1.3.8. Synthesis of Asp-linked hybrid 13 (IAN-5B). Prepared following the general diindolylation and deprotection procedure previously described for hybrids **10** and **11** using 5-iodo-1H-indole. Obtained as off-white solid. Yield: 19% (0.08 g, for two steps). ^{1}H NMR (400 MHz, acetone-d_6): δ (ppm) 10.34 (br s, 1H), 10.28 (br s, 1H), 7.55 (d, J = 8.2 Hz, 1H), 7.51–7.34 (m, 6H), 7.02 (t, J = 2.4 Hz, 2H), 7.0 (t, J = 2.4

Hz, 2H), 4.67 (q, J = 5.0 Hz, 1H), 4.58–4.45 (m, 1H), 3.51–3.48 (m, 1H), 2.89–2.77 (m, 1H), 2.61–2.53 (m, 1H), 2.39–2.29 (m, 1H), 2.24–2.12 (m, 1H), 1.94–1.85 (m, 1H), 1.92–1.73 (m, 5H), 1.64–1.54 (m, 2H), 1.50–1.31 (m, 9H), 1.29–1.02 (m, 8H), 0.98–0.90 (m, 7H), 0.66 (s, 3H); ^{13}C NMR (100 MHz, acetone-d_6): δ (ppm) 175.3, 174.7, 136.8, 136.7, 129.3, 129.0, 126.0, 125.0, 124.8 (2C), 122.4, 122.4, 119.6, 119.6, 119.3, 117.8, 114.0, 113.9, 72.08, 57.6, 57.2, 52.2, 43.7, 43.3, 41.6, 41.3, 38.2, 37.5, 36.9, 36.6, 36.5, 35.6, 33.9, 33.0, 32.0, 31.6, 29.3, 28.3, 27.6, 25.2, 24.2, 21.8, 19.2, 12.8; **HRMS** (ESI) calculated for C$_{44}$H$_{54}$N$_3$O$_4$Cl$_2$ (M–H)$^-$, 758.3497; found, 758.3502. HPLC purity: 97%.

4.1.3.9. Synthesis of Asp-linked hybrid 14. Prepared following the general diindolylation and deprotection procedure previously described for hybrids **10** and **11** using 5-fluoro-1H-indole. Obtained as off-white solid. Yield: 22% (0.07 g, for two steps). ^{1}H NMR (400 MHz, acetone-d_6): δ (ppm) 10.24 (br s, 1H), 10.18 (br s, 1H), 6.82 (d, J = 3.2 Hz, 1H), 7.45–7.13 (m, 6H), 6.86–6.78 (m, 2H), 4.74–4.45 (m, 2H), 3.58–3.50 (m, 1H), 2.78–2.64 (m, 1H), 2.61–2.53 (m, 1H), 2.37–2.28 (m, 1H), 2.23–2.11 (m, 1H), 2.02–1.95 (m, 1H), 1.91–1.72 (m, 5H), 1.64–1.45 (m, 4H), 1.44–1.24 (m, 10H), 1.21–1.03 (m, 5H), 0.98–0.90 (m, 7H), 0.65 (s, 3H); ^{13}C NMR (100 MHz, acetone-d_6): δ (ppm) 175.3, 174.8, 159.4, 159.3, 157.1, 157.0, 135.0, 134.8, 128.5, 128.4, 128.2, 128.1, 126.2, 125.2, 119.7, 119.6, 118.1, 118.1, 113.5, 113.4, 113.4, 113.3, 110.5, 110.2, 105.2, 105.1, 104.9, 104.8, 72.1, 57.6, 57.2, 52.3, 43.7, 43.3, 41.6, 41.3, 38.0, 37.5, 37.0, 36.6, 33.9, 33.0, 32.2, 31.5, 29.2, 28.3, 27.5, 25.2, 24.2, 19.2, 12.8. C–F splitting present; ^{19}F **NMR**: δ (ppm) −126.8, −126.9; **HRMS** (ESI) calculated for C$_{44}$H$_{54}$N$_3$O$_4$ (M − H)$^-$, 726.4088; found, 726.4096. HPLC purity: >99%.

4.1.3.10. Synthesis of Asp-linked hybrid 15. Prepared following the general diindolylation and deprotection procedure previously described for hybrids **10** and **11** using 5-methoxy-1H-indole. Obtained as off-white solid. Yield: 42% (0.17 g, for two steps). ^{1}H NMR (400 MHz, DMSO-d_6): δ (ppm) 12.35 (b, 1H), 10.66 (br s, 1H), 10.61 (br s, 1H), 8.21 (d, J = 7.67 Hz, 1H), 7.28–6.65 (m, 8H), 4.50–4.40 (m, 2H), 4.13–4.05 (m, 1H), 3.66 (d, J = 2.2 Hz, 6H), 3.43–3.35 (m, 2H), 2.69–2.60 (m, 1H), 2.43–2.35 (m, 1H), 2.32–2.27 (m, 1H), 2.02–1.91 (m, 2H), 1.87–1.65 (m, 4H), 1.56–1.32 (m, 8H), 1.28–1.13 (m, 7H), 1.12–0.98 (m, 4H), 0.96–0.86 (m, 7H), 0.62 (s, 3H); ^{13}C NMR (100 MHz, DMSO-d_6): δ (ppm) 174.8, 172.6, 152.6, 152.5, 131.9, 131.7, 127.0, 126.9, 123.4, 122.6, 118.2, 116.5, 111.9, 111.8, 110.3, 101.6, 101.4, 69.9, 56.1, 55.7, 55.3, 55.3, 51.0, 42.3, 41.6, 36.8, 36.3, 35.4, 35.2, 35.0, 34.2, 32.4, 31.7, 30.7, 30.4, 30.3, 27.8, 26.9, 26.2, 23.9, 23.3, 20.5, 18.4, 11.9 (some peaks overlapped with the solvent peak.); **HRMS** (ESI) calculated for C$_{46}$H$_{60}$N$_3$O$_6$ (M − H)$^-$, 750.4488; found, 750.4493. HPLC purity: >99%.

4.1.3.11. Synthesis of Asp-linked hybrid 16. Prepared following the general diindolylation and deprotection procedure previously described for hybrids **10** and **11** using 5-(benzyloxy)-1H-indole (see SI). Obtained as off-white solid. Yield: 51% (0.29 g, for two steps). ^{1}H NMR (400 MHz, acetone-d_6): δ (ppm) 9.94

(br s, 1H), 9.87 (br s, 1H), 7.50–7.15 (m, 17H), 6.84–8.73 (m, 2H), 5.15–4.90 (m, 4H), 4.65 (q, J = 4.9 Hz, 1H), 4.57 (m, 1H), 3.60–3.52 (m, 1H), 2.89–2.81 (m, 1H), 2.65–2.57 (m, 1H), 2.36–2.28 (m, 1H), 2.18–2.10 (m, 1H), 1.97–1.90 (m, 1H), 1.89–1.70 (m, 5H), 1.66–1.58 (m, 1H), 1.55–1.22 (m, 12H), 1.20–0.97 (m, 6H), 0.96–0.88 (m, 7H), 0.62 (s, 3H); **^{13}C NMR** (100 MHz, acetone-d_6): δ (ppm) 174.6, 174.4, 153.4, 153.3, 139.0 (2C), 133.4, 133.3, 129.1 (4C), 128.5 (4C), 128.4 (3C), 128.3, 124.4, 123.5, 119.5, 118.1, 112.8, 112.7 (2C), 112.6, 103.9, 103.9, 71.7, 71.2, 71.2, 57.2, 56.9, 52.3, 43.4, 43.0, 41.2, 40.9, 38.1, 37.3, 36.6, 36.3, 36.3, 36.2, 35.3, 33.7, 32.7, 31.8, 31.3, 28.9, 28.0, 27.2, 24.9, 23.9, 21.5, 18.9, 12.4; **HRMS** (ESI) calculated for $C_{58}H_{68}N_3O_6$ (M − H)$^-$, 902.5114; found, 902.5107. HPLC purity: >99%.

4.1.3.12. Synthesis of Asp-linked hybrid 17. Prepared following the general diindolylation and deprotection procedure previously described for hybrids **10** and **11** using 5-tert-butyl (1H-indol-5-yl) carbamate (see SI). Obtained as off-white solid. Yield: 74% (0.38 g, for two steps). **^{1}H NMR** (400 MHz, acetone-d_6): δ (ppm) 9.94 (br s, 1H), 9.87 (br s, 1H), 8.81–7.68 (m, 4H), 7.46–7.12 (m, 7H), 4.69–4.48 (m, 2H), 3.62–3.50 (m, 1H), 2.90–2.80 (m, 1H), 2.65–2.54 (m, 1H), 2.40–2.30 (m, 1H), 2.24–2.13 (m, 1H), 1.98–1.71 (m, 6H), 1.66–1.54 (m, 2H), 1.53–1.44 (m, 20H), 1.40–1.20 (m, 10H), 1.17–0.99 (m, 5H), 0.98–0.88 (m, 7H), 0.63 (s, 3H). **^{13}C NMR** (100 MHz, acetone-d_6): δ (ppm) 174.7, 174.4, 154.3, 154.3, 134.7134.5, 131.8, 131.8, 127.8, 124.3, 123.5, 119.5, 118.0, 115.7, 112.0, 111.9, 110.5, 110.2, 79.2, 79.2, 71.7, 57.2, 56.8, 52.4, 43.4, 43.0, 41.2, 40.9, 38.2, 37.2, 36.9, 36.3, 35.3, 33.4, 32.5, 31.9, 31.3, 28.9, 28.8 (6C), 28.7 (3C), 28.0, 27.2, 24.9, 23.9, 21.5, 18.9, 12.4; **HRMS** (ESI) calculated for $C_{54}H_{74}N_5O_8$ (M − H)$^-$, 920.5543; found, 920.5543. HPLC purity: >99%.

4.1.3.13. Synthesis of Asp-linked hybrid 18 (IAN-15B). Prepared following the general diindolylation and deprotection procedure previously described for hybrids **10** and **11** using 5-azido-1H-indole (see SI). Obtained as beige solid. Yield: 41% (0.18 g, for two steps). **^{1}H NMR** (400 MHz, acetone-d_6): δ (ppm) 10.31 (br s, 1H), 10.25 (br s, 1H), 7.63 (d, J = 8.0 Hz, 1H), 7.43–7.14 (m, 6H), 6.82–6.75 (m, 2H), 4.69 (q, J = 5.0 Hz, 1H), 4.60–4.52 (m, 1H), 3.61–3.51 (m, 1H), 2.90–2.80 (m, 1H), 2.69–2.52 (m, 1H), 2.40–2.30 (m, 1H), 2.25–2.14 (m, 1H), 1.98–1.62 (m, 1H), 1.90–1.71 (m, 5H), 1.67–1.59 (m, 1H), 1.55–1.40 (m, 4H), 1.39–1.30 (m, 6H), 1.26–0.98 (m, 8H), 0.95–0.86 (m, 7H), 0.63 (s, 3H); **^{13}C NMR** (100 MHz, acetone-d_6): δ (ppm) 174.5, 174.0, 135.6, 135.4, 131.0, 130.9, 128.4, 128.2, 125.2, 124.2, 118.9, 117.4, 113.5, 113.4, 113.4, 113.2, 109.5, 109.5, 71.4, 57.0, 56.6, 51.7, 51.6, 43.1, 42.7, 41.0, 40.7, 37.5, 36.9, 36.4, 35.9, 35.0, 33.3, 32.4, 31.4, 31.0, 28.6, 27.7, 26.9, 24.5, 23.6, 21.2, 18.6, 12.1; **HRMS** (ESI) calculated for $C_{44}H_{54}N_9O_4$ (M − H)$^-$, 772.4304; found, 772.4310. HPLC purity: >99%.

4.1.4 Molecular docking studies. For the molecular docking studies, the crystal structure of human ST6GAL1 (PDB ID: 6QVT) was obtained from the Protein Data Bank and prepared using UCSF Chimera and AutoDock Tools.[52,53] The ligand structures of **IAN-5B** and **IAN-15B** were similarly prepared using AutoDock Tools. The docking region was defined using the following parameters – the grid box was centered at coordinates 19.41, 28.16, and 78.68, with dimensions of 80, 80, and 80 grid points along the X, Y, and Z axes, respectively, and a grid spacing of 0.375 Å. These settings ensured adequate coverage of both the sugar acceptor and CMP-Neu5Ac binding sites for accurate ligand–receptor interaction analysis. Docking simulations were carried out using AutoDock4,[52] employing the Lamarckian Genetic Algorithm with 150 independent runs. The binding energy values obtained from the docking simulations were recorded for each ligand. The highest-ranked poses were analyzed and visualized using DS Visualizer to identify key molecular interactions towards the ST isozyme.

4.2 Biology

4.2.1 General remarks. All LCA-DIM hybrids were evaluated for their inhibitory activity against two sialyltransferase (ST) representatives: N-glycan α2,6-ST6GAL1 and O-glycan α2,3-ST3GAL1, using a UPLC-based ST inhibition assay following a previously reported protocol.[24] Human ST6GAL1 enzyme (R&D Systems, #7620-GT) with a specific activity >150 pmol min^{-1} µg^{-1} was acquired, stored at −80 °C, and utilized within three months of purchase. Rat ST3GAL1 (Calbiochem, #566227) was also obtained, with reported specific activities of 2.4 and 7.0 U mg^{-1}. It was similarly stored at −80 °C and used within a three-month period. The donor substrate CMP-Neu5Ac (Sigma, #C8271), along with the acceptor substrates Galβ1-4GlcNAc (N-acetyllactosamine, Calbiochem/Millipore, #345250) and p-nitrophenyl T-antigen (Calbiochem, #575303), were sourced from commercial suppliers.

All cells used for the cell-based assays were purchased commercially. The human breast carcinoma cell line MDA-MB-231 was obtained from the Bioresource Collection and Research Center (BCRC 60425). The other two TNBC cell lines, BT549 (HTB-122) and Hs578T (HTB-126), were acquired from the American Type Culture Collection (ATCC). HUVEC were obtained from Lonza (#C2519A). All cells were cultured in DMEM medium supplemented with 10% fetal bovine serum (FBS) under humidified conditions at 37 °C with 5% CO_2.

4.2.2 UPLC-based sialyltransferase inhibition assay. For the ST3GAL1 inhibition assay, reaction mixtures were prepared in a final volume of 50 µL containing 200 mM MES buffer, 100 mM NaCl, 0.5 mM EDTA, 0.01% Triton X-100, 1.4 µg of ST3GAL1 enzyme, 2.5 mM p-nitrophenyl T-antigen as the acceptor substrate, 1 mM CMP-Neu5Ac as the donor substrate, and test hybrids adjusted to a final concentration of 500 µM. For the ST6GAL1 assay, each 50 µL reaction contained 25 mM Tris buffer, 150 mM NaCl, 5 mM $CaCl_2$, 10 mM $MnCl_2$, 0.5 µg of ST6GAL1, 25 µM Galβ1-4GlcNAc as the acceptor, 1 mM CMP-Neu5Ac, and hybrids at a final concentration of 25 µM.

All reactions were incubated at 37 °C for 15 minutes, followed by thermal inactivation at 101 °C for 10 minutes. The resulting sialylated products were quantified via UPLC analysis to assess inhibitory activity. For IC_{50} determination,

selected compounds were tested across 5 to 8 different concentrations, spanning the full range of inhibition (0–100%). Residual enzymatic activity was normalized using an internal standard, and the inhibition curves were plotted against inhibitor concentration. IC_{50} values were calculated by fitting the data to a sigmoidal dose–response model (4-parameter logistic model) using GraphPad Prism. Enzyme kinetics were further evaluated by applying nonlinear regression to the initial rate data.

4.2.3 MTT assay. Approximately 10 000 TNBC (MDA-MB-231, BT549, and Hs578T) cells were seeded into 96-well plates and treated with varying concentrations of 3,3-DIM and the LCA-DIM hybrids ranging from 0.5–80 μM. The cells were then incubated for 48 h, with a 0.1% DMSO-containing medium used as a control. Following incubation, MTT reagent (1 mg mL^{-1}; Sigma) was added, and cells were further incubated at 37 °C for 4 hours to allow for formazan crystal formation. The medium was then replaced with DMSO to solubilize the crystals, and plates were kept at room temperature for 30 minutes. Absorbance was measured at 540 nm using a Molecular Devices SPECTRAmax PLUS384 microplate reader to assess the cytotoxicity of the test compounds.

4.2.4 Transwell migration assay. For initial migration screening, transwell chambers equipped with 8.0 μm pore-size filter inserts were used. MDA-MB-231 cells (8×10^4) were seeded into the upper chambers and treated with 80 μM of LCA-DIM hybrids or 3,3'-DIM, while cells treated with DMSO served as the control group. SFM was also utilized as control to ensure the reproducibility of the assay. For further evaluation across other TNBC cell lines, the transwell migration assay was performed using two additional cell lines BT549 and Hs578T and were tested at concentrations of 40 and 80 μM. The lower chambers were filled with culture medium containing 5% fetal bovine serum (FBS) to act as a chemoattractant. After 16 h of incubation, migrated cells on the lower side of the membrane were fixed and stained with Giemsa solution. Migratory activity was assessed by counting stained cells under a microscope. All experiments were performed in triplicate.

4.2.5 HUVEC tube formation assay. Forty-eight-well plates were coated with Matrigel Basement Membrane Matrix (Corning) and allowed to polymerize for 30 minutes in a humidified atmosphere containing 5% CO_2 at 37 °C. Suspensions of HUVEC at a density of 6×10^4 cells per well were prepared in EGM-2 medium supplemented with 2% FBS and treated with various concentrations of compound 4e. The cells were incubated for 18 h at 37 °C in a humidified incubator with 5% CO_2. Tube formation was observed using an Olympus IX83 optical microscope and documented through photography. All experiments were performed in triplicate.

4.2.6 Lectin affinity assay and IP-Western blotting of captured integrin subunits. The protocol used for the lectin affinity assay was performed following a previously published protocol.[25] To isolate the α2,6-sialylated cell surface proteins, biotinylated SNA lectin (Vector Laboratories, Inc., Newark, CA, USA) was incubated with 1 mg of total cell lysate under gentle rotation at 4 °C for 16 hours. After binding, the lectin–

protein complexes were pulled down using streptavidin-conjugated agarose beads. Unbound proteins were removed by washing the beads three times with RIPA buffer, and the bound proteins were subsequently eluted with SDS-PAGE sample buffer. The eluted samples were then subjected to Western blot analysis using antibodies targeting integrin-β1, -β3, and -β4 (Integrin Antibody Sampler Kit, #4749, Cell Signaling Technology, Danvers, MA, USA). Band intensities were quantified using ImageJ software, and the resulting values were used to determine the ratio of integrin expression in treated samples relative to the control.

Author contributions

C. A. P. Concio - methodology, investigation, validation, visualization, formal analysis, writing – original draft; Y. T. He - methodology, investigation, validation; S. J. L. P. Perez - methodology, formal analysis, writing – review & editing; T. T. Chang - investigation, formal analysis, visualization; C. L. Cheng - investigation, formal analysis, visualization; S. D. Arco - supervision, project administration; W. S. Li - supervision, project administration, funding acquisition, writing – review & editing.

Conflicts of interest

There are no conflicts to declare.

Data availability

Supplementary information is available: The SI contains – synthesis methods for selected indoles, MTT data, Transwell migration data, IC_{50} plots, western blots analyses, NMR and Mass spectra, and HPLC profiles. See DOI: **https://doi.org/10.1039/D5MD00390C**.

The data supporting this article have been included as part of the SI.

Acknowledgements

References

1 C. Traving and R. Schauer, *Cell. Mol. Life Sci.*, 1998, **54**, 1330–1349.

2 S. Ghosh, in *Sialic Acids and Sialoglycoconjugates in the Biology of Life, Health and Disease*, ed. S. Ghosh, Academic Press, 2020, pp. 1–61.

3 C. Dobie and D. Skropeta, *Br. J. Cancer*, 2021, **124**, 76–90.

4 J. Du, S. Hong, L. Dong, B. Cheng, L. Lin, B. Zhao, Y.-G. Chen and X. Chen, *J. Biol. Chem.*, 2015, **290**, 12000–12013.

5 M. Hugonnet, P. Singh, Q. Haas and S. von Gunten, *Front. Immunol.*, 2021, **12**, 1–16.

6 S. Pietrobono and B. Stecca, *Cancers*, 2021, **13**, 2014.

7 F. Li and J. Ding, *Protein Cell*, 2018, **10**, 550–565.

8 Y. Li and X. Chen, *Appl. Microbiol. Biotechnol.*, 2012, **94**, 887–905.

9 H. X. Cui, H. Wang, Y. Wang, J. Song, H. Tian, C. Xia and Y. Shen, *Oncol. Rep.*, 2016, **36**, 3317–3324.

10 N. C. Hait, A. Maiti, R. Wu, V. L. Andersen, C.-C. Hsu, Y. Wu, D. G. Chapla, K. Takabe, M. E. Rusiniak, W. Bshara, J. Zhang, K. W. Moremen and J. T. Y. Lau, *Cancer Gene Ther.*, 2022, **29**, 1662–1675.

11 X. Wu, J. Zhao, Y. Ruan, L. Sun, C. Xu and H. Jiang, *Cell Death Dis.*, 2018, **9**, 1102.

12 R. B. Jones, K. A. Dorsett, A. B. Hjelmeland and S. L. Bellis, *J. Biol. Chem.*, 2018, **293**, 5659–5667.

13 R. B. Jones, A. D. Silva, K. E. Ankenbauer, C. M. Britain, A. Chakraborty, J. A. Brown, S. W. Ballinger and S. L. Bellis, *Glycobiology*, 2023, **33**, 626–636.

14 N. Bhalerao, A. Chakraborty, M. P. Marciel, J. Hwang, C. M. Britain, A. D. Silva, I. E. Eltoum, R. B. Jones, K. L. Alexander, L. E. Smythies, P. D. Smith, D. K. Crossman, M. R. Crowley, B. Shin, L. E. Harrington, Z. Yan, M. M. Bethea, C. S. Hunter, C. A. Klug, D. J. Buchsbaum and S. L. Bellis, *JCI insight*, 2023, **8**, 1–23.

15 M. Pérez-Garay, B. Arteta, L. Pagès, R. de Llorens, C. de Bolòs, F. Vidal-Vanaclocha and R. Peracaula, *PLoS One*, 2010, **5**, e12524.

16 G. Venturi, I. Gomes Ferreira, M. Pucci, M. Ferracin, N. Malagolini, M. Chiricolo and F. Dall'Olio, *Glycobiology*, 2019, **29**, 684–695.

17 M. Smithson, R. Irwin, G. Williams, K. L. Alexander, L. E. Smythies, M. Nearing, M. C. McLeod, S. Al Diffalha, S. L. Bellis and K. M. Hardiman, *J. Biol. Chem.*, 2022, **298**, 1–7.

18 S. J. L. P. Perez, C.-W. Fu and W.-S. Li, *Molecules*, 2021, **26**, 5673.

19 R. Al Saoud, A. Hamrouni, A. Idris, W. K. Mousa and T. Abu Izneid, *Biomed. Pharmacother.*, 2023, **165**, 115091.

20 R. Szabo and D. Skropeta, *Med. Res. Rev.*, 2017, **37**, 219–270.

21 J.-Y. Chen, Y.-A. Tang, S.-M. Huang, H.-F. Juan, L.-W. Wu, Y.-C. Sun, S.-C. Wang, K.-W. Wu, G. Balraj, T.-T. Chang, W.-S. Li, H.-C. Cheng and Y.-C. Wang, *Cancer Res.*, 2011, **71**, 473–483.

22 K.-H. Chang, L. Lee, J. Chen and W.-S. Li, *Chem. Commun.*, 2006, 629–631, DOI: 10.1039/B514915K.

23 C.-H. Chiang, C.-H. Wang, H.-C. Chang, S. V. More, W.-S. Li and W.-C. Hung, *J. Cell. Physiol.*, 2010, **223**, 492–499.

24 C.-W. Fu, H.-E. Tsai, W.-S. Chen, T.-T. Chang, C.-L. Chen, P.-W. Hsiao and W.-S. Li, *J. Med. Chem.*, 2021, **64**, 527–542.

25 H.-E. Tsai, C.-L. Chen, T.-T. Chang, C.-W. Fu, W.-C. Chen, S. J. L. P. Perez, P.-W. Hsiao, M.-H. Tai and W.-S. Li, *Int. J. Mol. Sci.*, 2024, **25**, 4283.

26 S. J. L. P. Perez, C.-L. Chen, T.-T. Chang and W.-S. Li, *Bioorg. Med. Chem. Lett.*, 2024, **105**, 129760.

27 Y. Kang, Z.-T. Mai, L.-F. Yau, R.-F. Li, T.-T. Tong, C.-G. Yang, K.-M. Chan, Z.-H. Jiang, Y. Wang, Z.-F. Yang and J.-R. Wang, *J. Virol.*, 2022, **96**(6), 1–19.

28 K.-Y. Lee, H. G. Kim, M. R. Hwang, J. I. Chae, J. M. Yang, Y. C. Lee, Y. K. Choo, Y. I. Lee, S.-S. Lee and S.-I. Do, *J. Biol. Chem.*, 2002, **277**, 49341–49351.

29 A. P. Montgomery, C. Dobie, R. Szabo, L. Hallam, M. Ranson, H. Yu and D. Skropeta, *Bioorg. Med. Chem.*, 2020, **28**, 115561.

30 S. M. Kim, *Int. J. Mol. Sci.*, 2016, **17**, 1155.

31 E. J. Kim, M. Shin, H. Park, J. E. Hong, H.-K. Shin, J. Kim, D. Y. Kwon and J. H. Y. Park, *J. Nutr.*, 2009, **139**, 2373–2379.

32 Y. Jiang, Y. Fang, Y. Ye, X. Xu, B. Wang, J. Gu, M. Aschner, J. Chen and R. Lu, *Front. Pharmacol.*, 2019, **10**, 1–23.

33 S.-Y. Fang, S.-Y. Chen, Y.-Y. Chen, T.-J. Kuo, Z.-H. Wen, Y.-H. Chen, T.-L. Hwang and P.-J. Sung, *Nat. Prod. Commun.*, 2021, **16**, 1934578X211033735.

34 F. A. Wati, M. Santoso, Z. Moussa, S. Fatmawati, A. Fadlan and Z. M. A. Judeh, *RSC Adv.*, 2021, **11**, 25381–25421.

35 S. Chakraborty, S. Ghosh, B. Banerjee, A. Santra, A. Adhikary, A. K. Misra and P. C. Sen, *Front. Pharmacol.*, 2016, **7**, 1–21.

36 S.-M. Huang, P.-C. Hsu, M.-Y. Chen, W.-S. Li, S. V. More, K.-T. Lu and Y.-C. Wang, *Int. J. Cancer*, 2012, **131**, 722–732.

37 C.-H. Wang, C.-L. Chen, S. V. More, P.-W. Hsiao, W.-C. Hung and W.-S. Li, *PLoS One*, 2014, **9**, e101088.

38 B. H. Lipshutz and J. Keith, *Tetrahedron Lett.*, 1998, **39**, 2495–2498.

39 T. Fukuyama, S. C. Lin and L. Li, *J. Am. Chem. Soc.*, 1990, **112**, 7050–7051.

40 T. Miyazaki, Y. Han-ya, H. Tokuyama and T. Fukuyama, *Synlett*, 2004, **2004**, 477–480.

41 B. Biersack, *Cancer Drug Resist.*, 2020, **3**, 867–878.

42 O. D. Reyes-Hernández, G. Figueroa-González, L. I. Quintas-Granados, S. C. Gutiérrez-Ruíz, H. Hernández-Parra, A. Romero-Montero, M. L. Del Prado-Audelo, S. A. Bernal-Chavez, H. Cortés, S. I. Peña-Corona, L. Kiyekbayeva, D. A. Ateşşahin, T. Goloshvili, G. Leyva-Gómez and J. Sharifi-Rad, *Cancer Cell Int.*, 2023, **23**, 180.

43 S.-Y. Chen, P.-L. He, L.-Y. Lu, M.-C. Lin, S.-H. Chan, J.-S. Tsai, W.-T. Luo, L.-H. Wang and H.-J. Li, *Cancer Res.*, 2025, **85**, 1199–1218.

44 J. Lu, T. Isaji, S. Im, T. Fukuda, N. Hashii, D. Takakura, N. Kawasaki and J. Gu, *J. Biol. Chem.*, 2014, **289**, 34627–34641.

45 D. Harrus, A. Harduin-Lepers and T. Glumoff, *J. Struct. Biol.*, 2020, **212**, 107628.

46 W.-S. Chen, C. A. P. Concio, T.-T. Chang, C.-L. Chen, S. J. L. P. Perez and W.-S. Li, *Bioorg. Chem.*, 2025, **159**, 108401.

47 B. Kuhn, J. Benz, M. Greif, A. M. Engel, H. Sobek and M. G. Rudolph, *Acta Crystallogr., Sect. D:Biol. Crystallogr.*, 2013, **69**, 1826–1838.

48 S. J. L. P. Perez, Z.-F. Hsu, T.-T. Chang, C.-L. Chen and W.-S. Li, *Eur. J. Med. Chem.*, 2025, **292**, 117674.

49 T. Isaji, Y. Sato, T. Fukuda and J. Gu, *J. Biol. Chem.*, 2009, **284**, 12207–12216.

50 J. Liu, X. Dong, R. Xie, Y. Tang, A. M. Thomas, S. Li, S. Liu, M. Yu and H. Qin, *Placenta*, 2024, **149**, 18–28.

51 D. R. Christie, F. M. Shaikh, J. A. Lucas, J. A. Lucas and S. L. Bellis, *J. Ovarian Res.*, 2008, **1**, 3.

52 G. M. Morris, R. Huey, W. Lindstrom, M. F. Sanner, R. K. Belew, D. S. Goodsell and A. J. Olson, *J. Comput. Chem.*, 2009, **30**, 2785–2791.

53 E. F. Pettersen, T. D. Goddard, C. C. Huang, G. S. Couch, D. M. Greenblatt, E. C. Meng and T. E. Ferrin, *J. Comput. Chem.*, 2004, **25**, 1605–1612.